Journal of Computational Physics 228 (2009) 6536–6552

Contents lists available at ScienceDirect

Journal of Computational Physics

journal homepage: www.elsevier.com/locate/jcp

Adaptive rational spectral methods for the linear stability analysis of nonlinear fourth-order problems

Luis Cueto-Felgueroso *, Ruben Juanes

Department of Civil and Environmental Engineering, Massachusetts Institute of Technology, 77 Massachusetts Avenue, Cambridge, MA 02139, USA

ARTICLE INFO

Article history:
Received 21 January 2009
Received in revised form 27 May 2009
Accepted 28 May 2009
Available online 7 June 2009

Keywords:
Rational approximation
Spectral methods
Adaptivity
Linear stability analysis
Phase-field models
Thin films
Flow in porous media

ABSTRACT

This paper presents the application of adaptive rational spectral methods to the linear stability analysis of nonlinear fourth-order problems. Our model equation is a phase-field model of infiltration, but the proposed discretization can be directly extended to similar equations arising in thin film flows. The sharpness and structure of the wetting front preclude the use of the standard Chebyshev pseudo-spectral method, due to its slow convergence in problems where the solution has steep internal layers. We discuss the effectiveness and conditioning of the proposed discretization, and show that it allows the computation of accurate traveling waves and eigenvalues for small values of the initial water saturation/film precursor, several orders of magnitude smaller than the values considered previously in analogous stability analyses of thin film flows, using just a few hundred grid points.

1. Introduction

Fluid displacement fronts in porous media are often unstable. The rich variety of invasion patterns has been extensively characterized experimentally, and through simulations at the pore scale [67,23,55,85,56,68,58,43,69]. The classical macroscopic (continuum) models of multiphase flow in porous media, based on phase balance equations, generalizations of Darcy's law, and constitutive relationships for relative permeability and capillary pressure, are unable to explain these flow patterns in immiscible flow [38,79,65,1]. New macroscopic theories of flow of mixtures in porous media will emerge in the next few years, and most likely the mathematical structure of these new models will resemble that of models of phase transitions and surface growth [24]. One of the salient features of these advanced models is the presence of nonlinear, higher order terms, which require powerful numerical techniques for their discretization. This paper presents an example of such theoretical models, and an example of such specialized algorithms.

Gravity-driven infiltration of water into a homogeneous layer of soil is a simple and important case of pattern formation in multiphase flow in porous media. Rather than a compact infiltration front, the flow is often unstable and the water invasion takes the form of preferential flow paths (fingers). Intense experimental and theoretical work on the wetting front instability was initiated in the 70s [48,64,62], and has been followed by numerous measurements of finger formation and unstable gravity-driven infiltration (see, for example, [34,43,69,4,36,72,82,81]).

Despite overwhelming experimental evidence, the description of gravity-driven unsaturated flow using continuum balance laws has remained elusive. The traditional model, known as Richards' equation [66], is a mass balance equation in

* Corresponding author.
E-mail addresses: lcueto@mit.edu (L. Cueto-Felgueroso), juanes@mit.edu (R. Juanes).

0021-9991/$ - see front matter © 2009 Elsevier Inc. All rights reserved.
doi:10.1016/j.jcp.2009.05.045

which the water flux is modeled by a straightforward extension of Darcy's law to unsaturated media. It accounts for gravity, capillarity, and the fact that the permeability to water is reduced because the porous medium is only partially saturated with water. The inability of the Richards equation to explain fingered flow is well documented [35,33,51,78,36,38,37,79,61].

We have recently proposed a model of unsaturated flow that captures the relevant features of gravity fingering during infiltration [24]. The Richards model assumes, at least implicitly, that the system is homogeneous—gradients of water saturation are zero everywhere. Under this assumption, the free energy of the system is *local*, that is, it is a function of saturation only. Our model extends the description to a nonhomogeneous system, and explains the dynamics of unstable wetting fronts. The free energy is *nonlocal* (it is a function of water saturation and its gradient), and it leads to an additional term that is formally equivalent to an apparent surface tension at the wetting front: a nonlinear, fourth-order term. The model predicts a saturation overshoot at the tips of the fingers, a feature that is believed to be essential for the instability of the infiltration front [70,42,30,71,31]. The mathematical structure of the model is analogous to that describing the flow of thin films and driven contact lines [50,77,49,18,86,52,27,26,75,44,53], and to phase-field models of epitaxial growth of surfaces, binary transitions and solidification [21,22,19,40].

This paper discusses the numerical technology used for the linear stability analysis of our model of infiltration, which can be extended to perform analogous stability analyses of thin film flows. Fourth-order models arising in dynamic contact lines are demanding, because of the presence of steep fronts with nontrivial structure, and because the most interesting case corresponds to the degenerate limit (vanishing initial water saturation/precursor film thickness).

We argue that pseudo-spectral methods based on adaptive rational approximation are among the best choices for this type of problem. The first adaptive spectral methods based on parametrized maps include [6,47,7,54]. Rational interpolants have recently emerged as promising tools for the development of spectral methods for boundary-value problems [9,10,3,13,14,2,11,17,15,16,74,41,29]. Their success is partly due to their flexibility in the adaptive selection of nodes and poles [3,10,13–16,74,41,29]. Tee and Trefethen [74] have extended the rational spectral method of [2], which does not require that the underlying problem be transformed into new coordinates, and takes into account and locates a priori unknown singularities of the underlying solution. They use conformal mapping to design transformed nodes that improve the Chebyshev spectral method. Chebyshev–Padé approximation is used to approximate the locations of the singularities of the solution in the complex plane. We show that the proposed discretization allows us to compute accurate traveling waves and eigenvalues for very small values of the initial water saturation/film precursor, several orders of magnitude smaller than the values considered previously in analogous stability analyses of thin film flows [18,26,44], using just a few hundred grid points.

The paper is organized as follows: Section 2 presents the mathematical model and its nondimensional form. The base solutions about which the model equation will be linearized are traveling waves. They are introduced, together with the linearized problem, in Section 3. Section 4 presents a motivation for the adaptive algorithm, through the performance of standard collocation schemes. Section 5 introduces the adaptive rational approximation, and discusses practical implementation issues and the conditioning of differentiation matrices based on this type of approximation. Finally, Section 6 presents convergence results and examples of application to infiltration problems, and the main conclusions of our study are summarized in Section 7.

2. Mathematical model of gravity-driven infiltration

Consider constant-flux infiltration into a porous medium (Fig. 1). The evolution of the system is characterized in terms of the water saturation $S \in [0,1]$, that is, the locally-averaged fraction of the pore space occupied by water. It is assumed that the initial water saturation S_0 is uniform, and that the infiltration rate R_F is uniformly distributed and constant in time. The x-spatial coordinate points downwards, in the direction of gravity (acceleration g). The water density and dynamic viscosity are ρ and μ. The relevant macroscopic parameters concerning the porous medium are its intrinsic permeability k, and its porosity ϕ. The permeability of the medium is often expressed as a saturated hydraulic conductivity, $K_s = k\rho g/\mu$, which equals the gravity-driven flux under full saturation. Hence, the infiltration rate R_F may be expressed as a flux ratio, $R_s = R_F/K_s$, with $R_s \in [0,1]$. When this idealized flow scenario is simulated experimentally, the stability of the wetting front seems to be controlled by the flux ratio, initial saturation and material nonlinearity [39]. A saturation overshoot is observed at the tip of the fingers, which grow as traveling waves, advancing with constant velocity [70]. The formation of fingers appears as a winner-takes-all process, by which the fastest growing fingers in the initial unstable front channelize most of the infiltrating fluid and inhibit the growth of other incipient fingers [43,70]. The initial moisture content plays a critical role in the fingering instability: even relatively low saturations lead to a compact, downward-moving wetting front [59]. Stable fronts are also observed in dry media when the infiltration rate is either very small or approaches the saturated conductivity. In general, larger infiltration rates produce faster, thicker fingers [43].

2.1. Phase-field model of unsaturated flow

Under unsaturated conditions (water saturation S strictly less than one), it is well justified to make two assumptions [8,63]. First, air is infinitely mobile compared to water and, as a result, the air pressure remains constant and equal to the atmospheric pressure. Second, the compressibility of water and rock are negligible compared to that of air and, therefore, the water density ρ and the porosity ϕ are constant. Our model for the evolution of water saturation is [24,25]

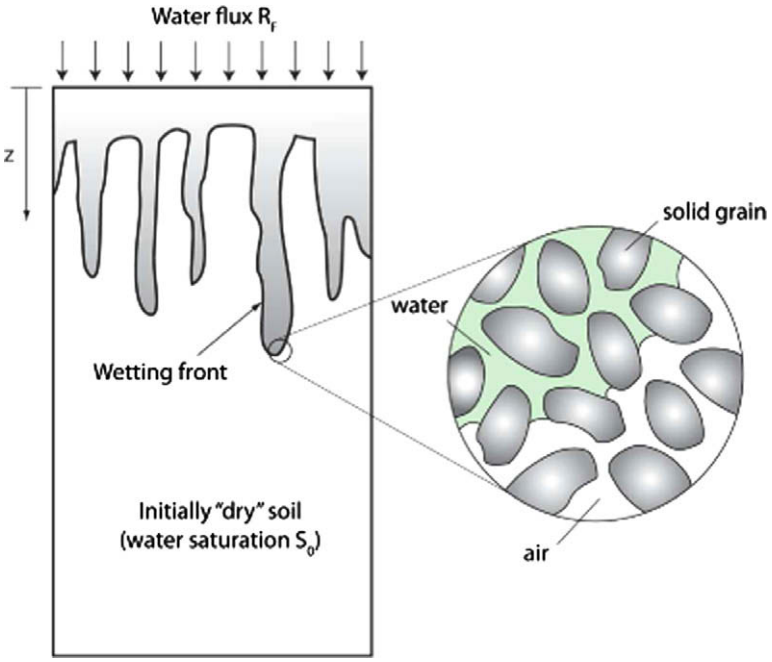

Fig. 1. Schematic of vertical infiltration of water into a porous medium. Initially, the soil is almost dry (water saturation S_0). A constant and uniformly distributed flux of water R_F ($\mathrm{L\,T^{-1}}$) is allowed to infiltrate into the soil. The flux of water is less than the hydraulic conductivity of the soil, K_s, so that the flux ratio $R_s = R_F/K_s < 1$. Macroscopically, a diffuse interface (the wetting front) moves downwards. This interface is often unstable and takes the form of long and narrow fingers that travel faster than the base of the wetting front (see, e.g. Fig. 2 in [43]). Microscopically, a sharp interface between water and air exists (see inset), which is locally governed by capillary effects. From [24]. Copyright American Physical Society.

$$\phi\frac{\partial S}{\partial t}+\nabla\cdot\left[\frac{k\rho g}{\mu}k_r(S)\left(\nabla x+\frac{1}{\rho g}\nabla P_c(S)+\frac{\Gamma}{\rho g}\nabla(\Delta S)\right)\right]=0. \tag{1}$$

The relative permeability k_r is an increasing and typically convex function of water saturation [66,8]. The capillary pressure $P_c(S)$ is a monotonically decreasing but nonconvex function of water saturation [8]. The coefficient Γ plays the role of an apparent surface tension associated with the wetting front [50,85,32]. Our model is an extension of the Richards equation; it deviates from the classical model through the introduction of a fourth-order term, which arises from honoring the inhomogeneity of the water–air–solid system in the definition of its free energy [24,25].

We nondimensionalize equation (1) by selecting a characteristic length scale, L, and a characteristic time, $T=\phi L\mu/(\rho g k)=\phi L/K_s$. The capillary pressure is expressed as:

$$P_c(S)=\rho g h_{\mathrm{cap}} J(S), \tag{2}$$

where $J(S)$ is a dimensionless capillary pressure function, and h_{cap} is the capillary rise, whose dependence on the system parameters is given by the Leverett scaling [57]:

$$h_{\mathrm{cap}}\sim\frac{\gamma\cos\theta}{\rho g\sqrt{k/\phi}}, \tag{3}$$

where γ is the surface tension between the fluids, and θ is the contact angle between the air–water interface and the solid surface [28].

We define the following two nondimensional groups:

$$N_{gr}=\frac{L}{h_{\mathrm{cap}}}\quad(\text{gravity number}), \tag{4}$$

$$N_{n\ell}=\frac{\Gamma}{\rho g L^3}\quad(\text{nonlocal or Cahn number}). \tag{5}$$

With these definitions, and understanding the space and time coordinates (x,t) as their dimensionless counterparts, the model reads:

$$\frac{\partial u}{\partial t}+\nabla\cdot\left[k_r(u)(\nabla x+N_{gr}^{-1}\nabla J(u)+N_{n\ell}\nabla(\Delta u))\right]=0, \tag{6}$$

where we have used $u \equiv S$ to emphasize that the problem is expressed in nondimensional form. The relative permeability and capillary pressure functions are chosen to fit experimental data from quasi-static experiments. In the following, we adopt the van Genuchten–Mualem model [60,80],

$$k_r(u) = \sqrt{u}\left[1 - (1 - u^{1/m})^m\right]^2, \tag{7}$$

$$J(u) = (u^{-1/m} - 1)^{1/n}, \tag{8}$$

where $m = 1 - 1/n$. This model introduces the material parameter n, which depends on how well-sorted the porous medium is [80].

2.2. Related models in fluid mechanics

Fourth-order spatial terms arise naturally in phase-field models with conserved order parameters [22,21,40]. Our model is also analogous to that describing the flow of thin fluid films sliding down an inclined plane. Adopting the lubrication approximation [46,50,77,49,18], the evolution equation of the film height h can be written as

$$3\mu\frac{\partial h}{\partial t} + \nabla \cdot [h^3(\rho g \sin(\alpha)\nabla x - \rho g \cos(\alpha)\nabla h + \gamma\nabla(\Delta h))] = 0, \tag{9}$$

where μ is the viscosity of the fluid, ρ its density, γ the fluid–air surface tension, and α the inclination angle of the plane (a vertical wall corresponds to $\alpha = \pi/2$). Gravity acts along the direction x. In dimensionless variables, the above equation reads [44]

$$\frac{\partial h}{\partial t} + \nabla \cdot [h^3(G_{\parallel}\nabla x - G_{\perp}\nabla h + \nabla(\Delta h))] = 0. \tag{10}$$

The dimensionless parameters $G_{\parallel}$ and $G_{\perp}$ are defined as

$$G_{\parallel} = \frac{L^3\rho g \sin(\alpha)}{h_c\gamma}, \quad G_{\perp} = \frac{L^2\rho g \cos(\alpha)}{\gamma}. \tag{11}$$

In the above expressions, L is an arbitrary reference length, and h_c is a reference height of the film. Note that the lubrication approximation yields an expression for the fluid velocity that resembles Darcy's law:

$$\mathbf{v} = -\frac{h^2}{\mu}\nabla p + h^2\rho g \sin(\alpha)\nabla x, \tag{12}$$

where the pressure is given by

$$p = -\gamma\Delta h + \rho g \cos(\alpha) h. \tag{13}$$

For completely wetting fluids, Troian et al. [77] proposed to model the contact line dynamics by assuming a precursor film of (small) thickness b downstream of the front. In our context, this precursor film corresponds to the initial water saturation.

The thin film Eq. (9) considers surface tension effects, and therefore gradient terms enter naturally in the free energy of the system. Note that surface tension has been identified as a fundamental physical mechanism to explain gravitational instabilities in thin film flows [50]. Conversely, by considering gradient terms in the free energy of the fluid–air–solid system, our model of infiltration (1) includes a new term that resembles an apparent (macroscopic) surface tension. Note that this apparent surface tension stems from the nonhomogeneity of the system, rather than from a sharp interface. Hence, we postulate [24] that the nondimensional group $N\ell$ should be expressed in terms of the physical parameters already considered in the Richards model. We arrive at the scaling $N_{n\ell} \sim N_{gr}^{-3}$. More precisely, we propose

$$N_{n\ell} = N_{gr}^{-3}. \tag{14}$$

As a consequence, the gravity number N_{gr} sets the scale of the problem, and our model does not introduce new independent parameters with respect to the classical Richards equation.

3. Linear stability analysis

3.1. Traveling wave solutions

The basic states for the stability analysis of constant-flux infiltration are traveling wave solutions to (6), of the form

$$u(x, y, z, t) = u(\xi) = u(x - ct), \tag{15}$$

whose mere existence we conjecture, subject to the conditions at infinity

$$u|_{\xi\to-\infty} = u^-, \quad u|_{\xi\to+\infty} = u^+. \tag{16}$$

The wave speed c is given by

$$c = \frac{k_r(u^-) - k_r(u^+)}{u^- - u^+}. \tag{17}$$

Let us assume that all the derivatives of the traveling waves vanish as $\xi \to \pm\infty$. With gravity acting along the x-axis, the traveling wave solutions satisfy the ODE

$$-c\frac{du}{d\xi} + \frac{d}{d\xi}\left(k_r(u) + N_{gr}^{-1}k_r(u)J'\frac{du}{d\xi} + N_{n\ell}k_r(u)\frac{d^3u}{d\xi^3}\right) = 0. \tag{18}$$

Integrating once, and imposing the necessary conditions at infinity, we arrive at

$$-c(u-u^-) + k_r(u) - k_r(u^-) + N_{gr}^{-1}k_r(u)J'\frac{du}{d\xi} + N_{n\ell}k_r(u)\frac{d^3u}{d\xi^3} = 0, \tag{19}$$

with boundary conditions

$$u|_{\xi\to-\infty} = u^-, \quad u|_{\xi\to+\infty} = u^+, \quad \left.\frac{du}{d\xi}\right|_{\xi\to-\infty} = 0. \tag{20}$$

In practical applications, the asymptotic left state u^- is expressed as a flux ratio, $R_s = k_r(u^-)$, and the asymptotic right state u^+ denotes an initial water saturation of the porous medium, S_0.

3.2. Linearized flow equation

Consider perturbations of the base traveling wave solutions u_0 developed in the previous section, of the form

$$u(x,y,t) = u_0 + \epsilon g(x,y,t), \tag{21}$$

where $g(x,y,t)$ is a generic two-dimensional perturbation of order $O(1)$ and $\epsilon \ll 1$. Introducing the above perturbed solution in (6), and retaining terms that are at most $O(\epsilon)$, the evolution equation for the perturbation is, to first order in ϵ,

$$\frac{\partial g}{\partial t} + \frac{\partial}{\partial x}(k_r'g) + N_{gr}^{-1}\nabla\cdot\left[k_rJ'\nabla g + k_rJ''g\nabla u_0 + k_r'J'g\nabla u_0\right] + N_{n\ell}\nabla\cdot\left[k_r\nabla\Delta g + k_r'g\nabla\Delta u_0\right] = 0 \tag{22}$$

where it is understood that $k_r = k_r(u_0)$, $k_r' = k_r'(u_0)$, $J' = J'(u_0)$, and $J'' = J''(u_0)$. For convenience, let us use the notation

$$\begin{aligned} T_1 &= N_{gr}^{-1}\nabla\cdot[k_rJ'\nabla g + k_rJ''g\nabla u_0 + k_r'J'g\nabla u_0], \\ T_2 &= N_{n\ell}\nabla\cdot[k_r\nabla\Delta g + k_r'g\nabla\Delta u_0]. \end{aligned} \tag{23}$$

The above expressions can be rearranged as

$$T_1 = N_{gr}^{-1}\left[g\nabla\cdot(k_rJ''\nabla u_0 + k_r'J'\nabla u_0) + (\nabla(k_rJ') + k_rJ''\nabla u_0 + k_r'J'\nabla u_0)\cdot\nabla g + k_rJ'\Delta g\right], \tag{24}$$

and

$$T_2 = N_{n\ell}\left[g\nabla\cdot(k_r'\nabla\Delta u_0) + (k_r'\nabla\Delta u_0)\cdot\nabla g + (\nabla k_r)\cdot(\nabla\Delta g) + k_r\nabla\cdot(\nabla\Delta g)\right]. \tag{25}$$

Note that the base solution is constant along the y axis; i.e. $u_0 = u_0(\xi)$, where $\xi = x - ct$. Therefore $u_0 = u_0(x)$ in a reference frame moving with the speed c, and (24) and (25) can be rearranged as

$$T_1 = N_{gr}^{-1}\left[g\frac{d}{dx}\left(k_rJ''\frac{du_0}{dx} + k_r'J'\frac{du_0}{dx}\right) + \left(\frac{d}{dx}(k_rJ') + k_rJ''\frac{du_0}{dx} + k_r'J'\frac{du_0}{dx}\right)\frac{\partial g}{\partial x} + k_rJ'\Delta g\right], \tag{26}$$

and

$$T_2 = N_{n\ell}\left[g\frac{d}{dx}\left(k_r'\frac{d^3u_0}{dx^3}\right) + \left(k_r'\frac{d^3u_0}{dx^3}\right)\frac{\partial g}{\partial x} + \frac{dk_r}{dx}\left(\frac{\partial^3 g}{\partial x^3} + \frac{\partial^3 g}{\partial x\partial y^2}\right) + k_r\left(\frac{\partial^4 g}{\partial x^4} + 2\frac{\partial^4 g}{\partial x^2\partial y^2} + \frac{\partial^4 g}{\partial y^4}\right)\right]. \tag{27}$$

Within the aforementioned reference frame, and transforming to Fourier space in the y direction, the evolution equation for the y-transformed perturbation $G(x,\omega,t)$ is given by

$$\frac{\partial G}{\partial t} + G\frac{dk_r'}{dx} + \frac{\partial G}{\partial x}(k_r' - c) + \widehat{T_1} + \widehat{T_2} = 0, \tag{28}$$

where

$$\widehat{T_1} = N_{gr}^{-1}\left[G\frac{d}{dx}\left(k_rJ''\frac{du_0}{dx} + k_r'J'\frac{du_0}{dx}\right) + \left(\frac{d}{dx}(k_rJ') + k_rJ''\frac{du_0}{dx} + k_r'J'\frac{du_0}{dx}\right)\frac{\partial G}{\partial x} + k_rJ'\frac{\partial^2 G}{\partial x^2} - \omega^2k_rJ'G\right], \tag{29}$$

and

$$\widehat{T_2} = N_{n\ell}\left[G\frac{d}{dx}\left(k_r'\frac{d^3u_0}{dx^3}\right) + \left(k_r'\frac{d^3u_0}{dx^3}\right)\frac{\partial G}{\partial x} + \frac{dk_r}{dx}\left(\frac{\partial^3 G}{\partial x^3} - \omega^2\frac{\partial G}{\partial x}\right) + k_r\left(\frac{\partial^4 G}{\partial x^4} - 2\omega^2\frac{\partial^2 G}{\partial x^2} + \omega^4 G\right)\right]. \tag{30}$$

Rearranging (28), we finally arrive at the linear evolution problem

$$\frac{\partial G}{\partial t} + A_4\frac{\partial^4 G}{\partial x^4} + A_3\frac{\partial^3 G}{\partial x^3} + A_2\frac{\partial^2 G}{\partial x^2} + A_1\frac{\partial G}{\partial x} + A_0 G = 0, \tag{31}$$

where

$$A_0 = \frac{d}{dx}\left[k_r' + N_{gr}^{-1}\left(k_r J''\frac{du_0}{dx} + k_r' J'\frac{du_0}{dx}\right) + N_{n\ell}k_r'\frac{d^3u_0}{dx^3}\right] - N_{gr}^{-1}\omega^2 k_r J' + N_{n\ell}\omega^4 k_r, \tag{32}$$

$$A_1 = (k_r' - c) + N_{gr}^{-1}\left(\frac{d}{dx}(k_r J') + k_r J''\frac{du_0}{dx} + k_r' J'\frac{du_0}{dx}\right) + N_{n\ell}\left(k_r'\frac{d^3u_0}{dx^3} - \omega^2\frac{dk_r}{dx}\right), \tag{33}$$

$$A_2 = N_{gr}^{-1}k_r J' - 2N_{n\ell}\omega^2 k_r, \tag{34}$$

$$A_3 = N_{n\ell}\frac{dk_r}{dx}, \tag{35}$$

$$A_4 = N_{n\ell}k_r. \tag{36}$$

3.3. Discrete operators

The properties of the linear operator in Eq. (31) determine the evolution of infinitesimal perturbations of the base traveling wave solutions u_0. The evolution Eq. (31) can be discretized in the coordinate direction x, and the stability of the linearized perturbed flow can be studied in terms of the resulting discrete linear problem. We adopt a collocation approach, which reduces to the construction of discrete differential operators (matrices) $\mathbf{D}_1$, $\mathbf{D}_2$, $\mathbf{D}_3$ and $\mathbf{D}_4$, such that

$$\begin{aligned}\mathbf{G}_1 &= \mathbf{D}_1\mathbf{G},\\ \mathbf{G}_2 &= \mathbf{D}_2\mathbf{G},\\ \mathbf{G}_3 &= \mathbf{D}_3\mathbf{G},\\ \mathbf{G}_4 &= \mathbf{D}_4\mathbf{G},\end{aligned} \tag{37}$$

where the grid functions $\{G_{\alpha j},\ j = 0,\ldots,N\}$ are to be understood in the sense of

$$G_{\alpha j} \approx \left.\frac{\partial^\alpha G}{\partial x^\alpha}\right|_{x=x_j}. \tag{38}$$

The semi-discrete linearized flow problem reads

$$\frac{d\mathbf{G}}{dt} = \mathbf{M}\mathbf{G}, \tag{39}$$

in terms of the linear, autonomous operator

$$\mathbf{M} = -(\mathbf{A}_4\mathbf{D}_4 + \mathbf{A}_3\mathbf{D}_3 + \mathbf{A}_2\mathbf{D}_2 + \mathbf{A}_1\mathbf{D}_1 + \mathbf{A}_0). \tag{40}$$

In the above expression, the matrices $\mathbf{A}_k$, $k = 0,\ldots,4$, are diagonal, and their entries result from the evaluation of the coefficients (32)–(36) at the grid points. It follows from (39) that, given a perturbation $G(x,\omega,0) = G_0(x,\omega)$, i.e. given the grid function $\{G_{0j},\ j = 0,\ldots,N\}$, the evolution of this perturbation can be compactly written as

$$\mathbf{G}(t) = e^{t\mathbf{M}}\mathbf{G}_0, \quad e^{t\mathbf{M}} = \sum_{k=0}^{\infty}\frac{t^k\mathbf{M}^k}{k!}. \tag{41}$$

We are interested in the growth/decay of solutions $\mathbf{G}(t)$ to the linear time-dependent problem (39)–(41). Asymptotically, the behavior of the system is driven by the eigenvalues of $\mathbf{M}$. More precisely

$$\lim_{t\to\infty} t^{-1}\log\|e^{t\mathbf{M}}\| = \beta(\mathbf{M}), \tag{42}$$

where $\beta(\mathbf{M})$ is the spectral abscissa of $\mathbf{M}$.

4. Motivation for adaptive discretizations

4.1. Sample traveling waves and structure of the wetting front

The linear stability analysis of the model Eq. (6) can be summarized in two steps:

1. For a given set of parameters (u^-, u^+, n, N_{gr} and $N_{n\ell}$), compute the traveling wave solution to (6), u_0, by solving the boundary-value problem (19) and(20).
2. Construct the discrete linear operator **M** (given by Eqs. (40), (31)–(35) and (36)), and determine its spectral properties.

Computing accurate eigenvalues of **M** requires that the traveling waves are very well resolved, which is difficult due to the sharpness and structure of the wetting front. This is illustrated in Fig. 2, where we show a typical traveling wave (A), displaying the saturation overshoot and steep wetting front. The initial water saturation is relatively low ($u^+ = 10^{-3}$). The other parameters are $u^- = 0.6,\ N_{gr} = 1,\ N_{n\ell} = 1$ and $n = 10$. The challenge is to resolve the front and the small-scale feature downstream of the apparent wetting front (B). The extent of this feature, h_f, roughly scales like $h_f \sim u^+$, which makes the problem stiff in the degenerate limit $u^+ \to 0$. Once the traveling wave has been computed, we may construct the discrete operator **M** for different wave numbers ω, and their associated spectral abscissae (growth factors), $\beta = \beta(\omega)$. This leads to dispersion curves like the one shown in Fig. 2C. Consistency of the computed traveling waves with the linearized problem requires $\beta(0) = 0$. This requirement can be used as a measure of the accuracy of the discretization. Fig. 2D shows some eigenvalues and ϵ-pseudo-spectra of **M**, for $\omega = 0.54$. We plot the contours $\epsilon = 10^{-1.5}, 10^{-2}, \ldots, 10^{-8}$.

4.2. Performance of standard collocation methods

We attempt to compute the traveling waves (step 1) and linear operators (step 2) in the above problem using standard discretization techniques. The Chebyshev pseudo-spectral method approximates functions $u(x)$ by truncated Chebyshev expansions,

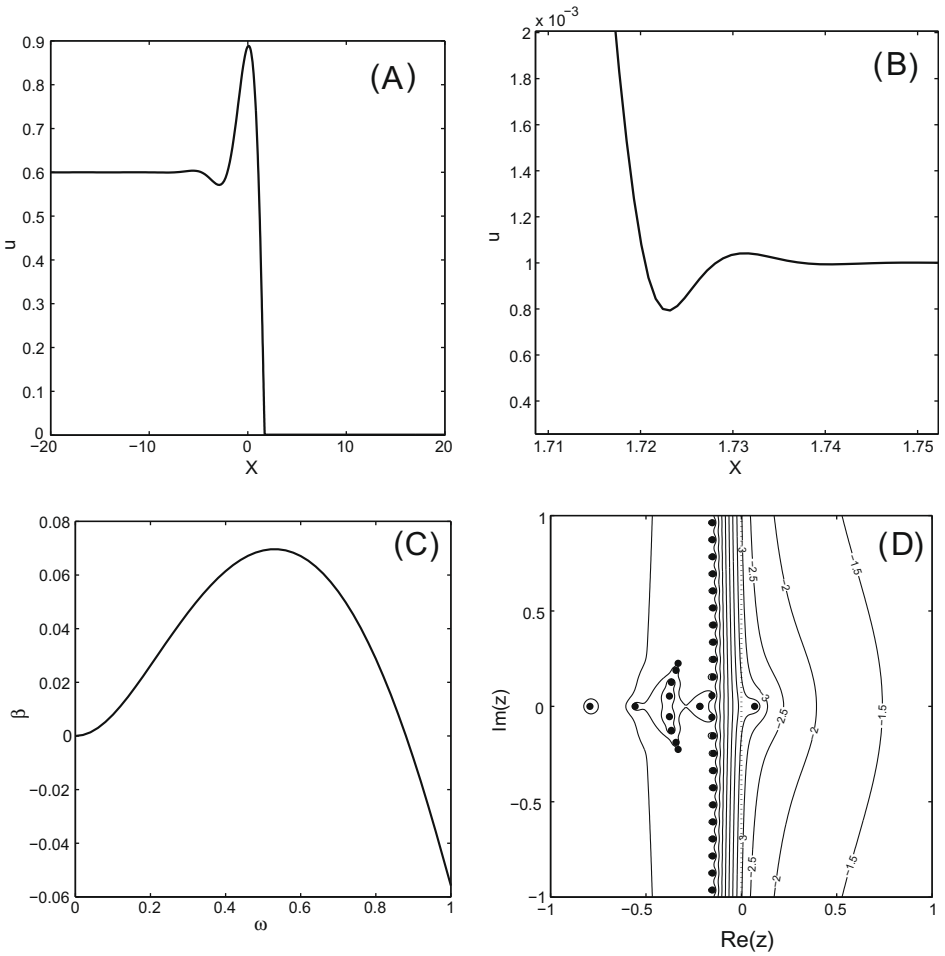

Fig. 2. (A) Sample traveling wave solution to (6). The model parameters are $u^- = 0.6,\ u^+ = 0.001,\ N_{gr} = 1,\ N_{n\ell} = 1$ and $n = 10$. (B) Close-up view of the small-scale feature at the wetting front. (C) Dispersion curve, plotting frequency ω against spectral abscissa (growth factor) β of matrix **M** (40). (D) Eigenvalues and ϵ-pseudospectra of **M**, for $\omega = 0.54$ (close-up view near the origin). We plot the contours $\epsilon = 10^{-1.5}, 10^{-2}, \ldots, 10^{-8}$.

$$u(x) \approx \sum_{j=0}^{N} a_j T_j(x), \quad T_j(x) = \cos(j \cos^{-1}(x)), \tag{43}$$

interpolating at the so-called Chebyshev nodes $x_j = \cos(j\pi/N), j = 0, \ldots, N$. The expansion coefficients in (43), $\{a_j\}$, are given by

$$a_0 = \frac{1}{\pi} \int_{-1}^{1} (1 - x^2)^{-1/2} f(x) dx, \tag{44}$$

$$a_j = \frac{2}{\pi} \int_{-1}^{1} (1 - x^2)^{-1/2} T_j(x) f(x) dx, \quad j = 1, \ldots, N. \tag{45}$$

With rows and columns indexed from 0 to N, the $(N+1) \times (N+1)$ Chebyshev differentiation matrix $\mathbf{D}^{Ch}$ has entries [76]

$$D_{jk}^{\mathrm{Ch}} = \begin{cases} \frac{c_j}{c_k} \frac{(-1)^{j+k}}{(x_j - x_k)}, & \text{if } j \neq k, \\ -\sum\limits_{l=0, l \neq k}^{N} D_{jl}^{\mathrm{Ch}}, & \text{if } j = k, \end{cases} \tag{46}$$

where

$$c_j = \begin{cases} 2, & j = 0 \text{ or } N, \\ 1, & \text{otherwise}. \end{cases} \tag{47}$$

For sufficiently smooth solutions, the approximation error in collocation schemes based on this discrete operator decays exponentially fast as $N \to \infty$. More precisely, if the solution can be continued as an analytic function in a closed ellipse with foci ± 1, semimajor axis length B, and semiminor axis length b, then the error behaves like $(B + b)^{-N}$ [76]. It follows from this result that, if the solution has singularities in the complex plane close to $[-1, 1]$, so that $B + b \approx 1$, then the convergence of the Chebyshev collocation method will be rather slow.

In the present context, this convergence behavior is illustrated in Fig. 3. We compute the traveling wave solutions to Eq. (6), obtained by solving the problem (19) and (20). The model parameters are $u^- = 0.6, N_{gr} = 1, N_{n\ell} = 1$ and $n = 10$. We compute solutions for various initial saturations, $u^- = 0.01, 0.04, 0.1$ and 0.2. As the initial water saturation is reduced, the Chebyshev collocation method becomes impractical (Fig. 3A), since very large values of N are required in order to resolve the sharp wetting front. The convergence of the spectrum of $\mathbf{M}$ for different values of u^+ reflects this trend (Fig. 3C). The slow convergence of Chebyshev expansions as $u^+ \to 0$ may be explained by looking at the singularities of the solution (Fig. 3B), which approach the real interval $[-1, 1]$ as $u^+ \to 0$ (only half of the singularities are shown; the others are symmetric with respect to the real line). Classical finite difference schemes also exhibit slow convergence when the degenerate limit is approached, as is shown in Fig. 3D for a centered, fourth-order finite difference discretization.

5. Adaptive rational collocation method

5.1. Rational approximation

Rational interpolants have recently emerged as promising tools for the development of spectral methods for boundary-value problems [2,11,16,74]. Their success is partly due to their flexibility in the adaptive selection of nodes and poles [3,10,13–16,74,41,29]. It is common to write the approximants in barycentric form [12,17], which provides a quite general framework that includes both polynomial and rational approximations. Thus, a rational function which interpolates a grid function $u_0, u_1, \ldots, u_N$ at points $x_0, x_1, \ldots, x_N$ can be expressed as

$$u(x) \approx r(x) = \frac{\sum_{k=0}^{N} \frac{w_k}{x - x_k} u_k}{\sum_{k=0}^{N} \frac{w_k}{x - x_k}}, \tag{48}$$

where $w_0, w_1, \ldots, w_N$ are called barycentric weights. In particular [17], the above expression is a polynomial that interpolates at the Chebyshev points $\{x_k = \cos(k\pi/N),\ k = 0, \ldots, N\}$ for

$$w_0 = \frac{1}{2}, \tag{49}$$

$$w_k = (-1)^k, \quad k = 1, \ldots, N - 1, \tag{50}$$

$$w_N = \frac{(-1)^N}{2}. \tag{51}$$

The pth derivative of r evaluated at x_j can be expressed as

$$r^{(p)}(x_j) = \sum_{k=0}^{N} D_{jk}^{(p)} u_k, \tag{52}$$

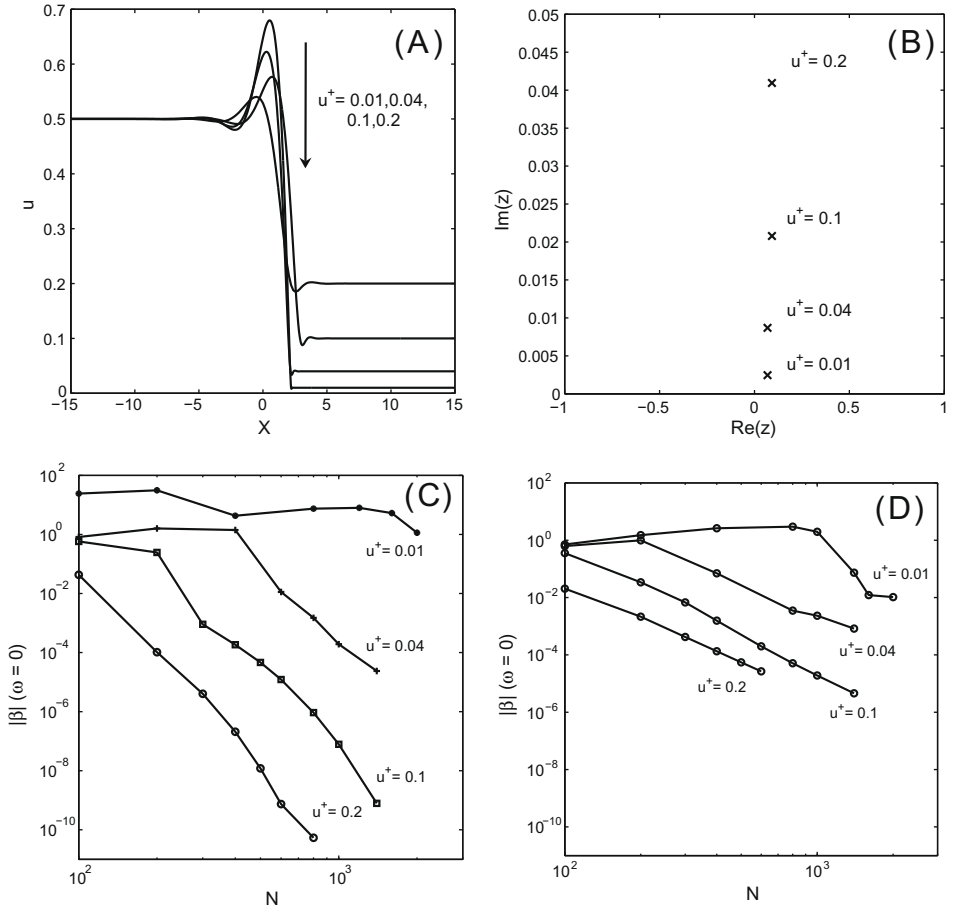

Fig. 3. Performance of standard collocation schemes in the linear stability analysis of (6). (A) Traveling wave solutions for various initial saturations, $u^- = 0.01, 0.04, 0.1$ and 0.2. The other parameters are $u^- = 0.5$, $N_{gr} = 1$, $N_{n\ell} = 1$ and $n = 10$. (B) Location of the singularities of the traveling waves. Only half of them are shown; the others are symmetric with respect to the real line. As the initial saturation is decreased, the singularities approach the real interval $[-1, 1]$, and the convergence of the Chebyshev spectral method is degraded, as shown in the convergence curves (C). (D) Same as (C), but using fourth-order centered differences.

in terms of the differentiation matrices $D^{(p)}_{jk}$. The first and second order differentiation matrices are [3]

$$D^{(1)}_{jk} = \begin{cases} \frac{w_k/w_j}{x_j - x_k}, & \text{if } j \neq k, \\ -\sum_{l=0, l\neq k}^{N} D^{(1)}_{jl}, & \text{if } j = k, \end{cases} \tag{53}$$

$$D^{(2)}_{jk} = \begin{cases} 2D^{(1)}_{jk}\left(D^{(1)}_{jj} - \frac{1}{x_j - x_k}\right), & \text{if } j \neq k, \\ -\sum_{l=0, l\neq k}^{N} D^{(2)}_{jl}, & \text{if } j = k. \end{cases} \tag{54}$$

Tee [73] has proposed the following formula to compute the entries of the nth order differentiation matrix,

$$D^{(n)}_{jk} = \begin{cases} \frac{n}{(x_j - x_k)}\left(\frac{w_k}{w_j} D^{(n-1)}_{jj} - D^{(n-1)}_{jk}\right), & \text{if } j \neq k, \\ -\sum_{l=0, l\neq k}^{N} D^{(n)}_{jl}, & \text{if } j = k, \end{cases} \tag{55}$$

where $D^{(0)}$ is the identity matrix.

5.2. Adaptive procedure

In [74], Tee and Trefethen present an elegant spectral collocation method that uses adaptively transformed Chebyshev nodes. Extending the method of [2], they use ideas proposed in [83] for the approximate location of singularities in the

complex plane, and conformal mapping in order to transform the Chebyshev grid into one that adaptively clusters points near steep gradients of the solution (singular lines). They successfully apply the algorithm to two evolution problems: a thermal blow-up problem (reaction–diffusion), and the viscous Burgers equation (a moving viscous shock). In both examples the sharp features of the solution evolve in time, and the explicit time marching allows for a smooth tracking of the singularities.

The basis of their method is the exponential convergence of rational approximations that interpolate at transformed Chebyshev nodes [3], i.e. rational approximations of the form

$$u_N(x) = \frac{\sum_{k=0}^{N}{}' \frac{(-1)^k}{x-x_k} u_k}{\sum_{k=0}^{N}{}' \frac{(-1)^k}{x-x_k}}, \quad x_k = g(\cos(k\pi/N)), \tag{56}$$

where the prime indicates that the first and last terms are halved, and the conformal map is denoted by g. Tee and Trefethen consider in [74] solutions with one relevant front to be resolved, and thus construct g using two singularities of the solution, $\delta \pm \epsilon i$, that are symmetric with respect to the real line. The proposed conformal map is

$$g(z) = \delta + \epsilon \sinh\left[\left(\sinh^{-1}\left(\frac{1-\delta}{\epsilon}\right) + \sinh^{-1}\left(\frac{1+\delta}{\epsilon}\right)\right)\frac{z-1}{2} + \sinh^{-1}\left(\frac{1-\delta}{\epsilon}\right)\right]. \tag{57}$$

In general, the singularities $\delta \pm \epsilon i$ are not known a priori, and have to be approximated numerically. Once the grid has been adapted as $x_k = g(\cos(k\pi/N))$, the rational interpolant (56) is used, following [2], as the basis for a collocation scheme, with differentiation matrices given by Eq. (55). Note that similar maps for solutions with multiple fronts have also been presented in [73].

5.3. Practical implementation issues

There are two critical aspects of the proposed adaptive strategy which may compromise its success in the present context (steady state, fourth-order nonlinear problem). Firstly, the grid adaptation is driven by the location of the singularities of the solution, which is not known a priori. Secondly, the presence of fourth-order derivatives raises the question about the conditioning of the discrete problem, and the possible relevance of finite precision effects. Also, in a more general context, Newton iterations have been identified as potentially unstable for the computation of traveling waves [20].

Finding the singularities of the numerical solution is a technical problem that soon becomes a practical one. The technical side is addressed in [74], following ideas from [83]: the singularities can be approximated by the poles of Chebyshev–Padé approximants. The practical problem is that, for the method to be effective, these approximants have to be representative of the solution at the sharp front themselves. As soon as the front has a nontrivial structure, as in our case of an equation with fourth-order terms, the location of the true singularity is easily missed and the adaptive scheme fails. Hence, until the front is not reasonably well resolved, there is much uncertainty about the real part of the singularities, δ (about the point around which the grid has to be refined). Note that we refer loosely to the singularities of the solution as $\delta \pm \epsilon i$, but no a priori knowledge of the singularity structure is required by the adaptive algorithm.

As a consequence of the initial uncertainty in δ, we use a continuation approach that progressively increases the level of clustering around the front; that is, we impose a restriction on the minimum value of ϵ that is allowed at each grid adaptation step. The condition numbers of the differentiation matrices grow very quickly with the node clustering, which imposes an absolute minimum value of ϵ that can be used in practice, ϵ_{min}. This minimum value of ϵ is due to conditioning rather than accuracy in resolving the front, which implies that the maximum accuracy that can be attained by the algorithm is reduced, due to conditioning problems, as the front becomes very sharp.

Following [74], the singularity location requires the definition of a local approximation of the solution, which is used to approximate the poles using the Chebyshev–Padé procedure. This is done by selecting an interval around the previously computed poles $\delta \pm \epsilon i$, as $I = [\delta - \xi, \delta + \xi]$, with $\xi = \min(10\epsilon, 1 - |\delta|)$. The solution is interpolated to the $M + 1$ Chebyshev points in I, and the singularity locator provides the new poles. The new value of ϵ is multiplied by a safety factor of 0.75. Following the continuation approach described above, we limit the minimum value of ϵ as $\epsilon = \max(\epsilon_0, \epsilon^*, \epsilon_{min})$, where ϵ_0 is the value provided by the Chebyshev–Padé singularity locator, ϵ^* is a reference value that is progressively decreased in the continuation process, and ϵ_{min} is a minimum limit value due to the explosive growth of the condition number of the differentiation matrices for small values of ϵ.

Taking into account the scaling of the characteristic length of the small-scale feature downstream of the wetting front, we have used the rule $\epsilon_{min} = Nu^+/500$ in the examples shown in this study. This formula should be modified to account for large changes in the flux ratio (u^-).

5.4. Conditioning of the differentiation matrices. finite precision effects

A known drawback on spectral methods is the fast growth of the condition number of differentiation matrices. More precisely, the condition number of Chebyshev differentiation matrices scales like N^{2k}, where k is the order of differentiation [84,5].

The conditioning of the differentiation matrices is approximately determined by how closely the grid points cluster. The scaling of the grid spacing near the boundaries is responsible for the fast growth of the condition number of the Chebyshev differentiation matrices. Decreasing the value of ϵ, the clustering parameter of the conformal map (57), alleviates the effects of clustering near the boundaries, thus improving the conditioning, but in turn clusters points around the front. Quite often, the grid size required to resolve the solution at the front is small enough to dominate the behavior of the condition number, which is larger than that of the un-mapped Chebyshev discretization.

Fig. 4 presents the normalized condition number of the first, second, third and fourth-order differentiation matrices (after imposing boundary conditions). The condition numbers are normalized with respect to those of the corresponding Chebyshev differentiation matrices. As ϵ is reduced, the conditioning improves with respect to Chebyshev approximation, until the clustering is actually more aggressive than that of Chebyshev grids, which results into an fast growth of the condition number as ϵ is reduced further. Note that these results apply to the conformal map (57), but may vary for different maps.

The practical consequence of this behavior is that ϵ cannot be arbitrarily small or, equivalently, that the maximum attainable accuracy decreases as the fronts become sharper. In the present context, the loss of accuracy is obvious as the initial saturation u^+ is reduced, as will be shown in Section 6.2 below.

6. Results

6.1. Convergence study

We present convergence results of standard collocation schemes (Chebyshev and finite differences), and of the adaptive rational spectral method, on the model problem

$$-c(u-u^-)+k_r(u)-k_r(u^-)+k_r(u)J'(u)\frac{du}{dx}+k_r(u)\frac{d^3u}{dx^3}=S(x). \tag{58}$$

We set $u^-=1$, and the constitutive relations

$$k_r(u)=u^3, \quad J(u)=u^{-1/4}. \tag{59}$$

The source term $S(x)$ is such that the exact solution is

$$u(x)=\frac{1}{2+\alpha}[1+\alpha-\tanh(\beta(x-x_\delta))], \tag{60}$$

which has an internal layer around x_δ. The asymptotic behavior of $u(x)$ is $u(-\infty)=1$ and $u(+\infty)=\alpha/(2+\alpha)$. In the present example we adopt $\alpha=0.01$. The parameter β, which is set as $\beta=100$, controls the characteristic thickness of the internal layer, which scales like β^{-1}, and $x_\beta=0.2$. We impose the boundary conditions

$$u|_{\xi\to-\infty}=u^-, \qquad u|_{\xi\to+\infty}=u^+, \qquad \left.\frac{du}{d\xi}\right|_{\xi\to-\infty}=0. \tag{61}$$

The problem is solved in $[-1,1]$ using three collocation schemes: centered, fourth-order finite differences, the Chebyshev pseudo-spectral method, and the above adaptive rational scheme. The different schemes are characterized by the grid $\{x_j\}$ and differentiation matrices, such that the discrete problem reads

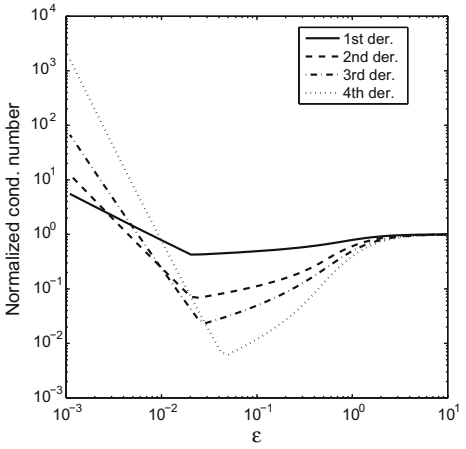

Fig. 4. Normalized condition number of the differentiation matrices as a function of the clustering parameter ϵ. The clustering is centered at $\delta=0$. The condition numbers are normalized with respect to those of the corresponding Chebyshev differentiation matrices.

$$\mathbf{R}(\mathbf{u}) = \mathbf{0}, \tag{62}$$

where

$$R_j = -c(u_j - u^-) + k_r(u_j) - k_r(u^-) + k_r(u_j)J'(u_j)\sum_{k=0}^{N} D^{(1)}_{jk}u_k + k_r(u_j)\sum_{k=0}^{N} D^{(3)}_{jk}u_k - S(x_j), \quad j = 0,\ldots,N.$$

We solve the nonlinear system of Eq. (62) using Newton iterations

$$\mathbf{u}^{p+1} = \mathbf{u}^p + \Delta\mathbf{u}^p, \quad \mathbf{J}(\mathbf{u}^p)\Delta\mathbf{u}^p = -\mathbf{R}(\mathbf{u}^p). \tag{63}$$

Denoting $K = k_r(u)J'(u), dK = K'(u)$ and $dkr = k_r'(u)$, where the prime denotes differentiation with respect to u, the Jacobian matrix $\mathbf{J}(\mathbf{u})$ can be compactly given using Matlab pseudo-code

```
>> J = diag(-c + dkr - dK.*(Dl * u) + dkr.*(D3 * u))...
   - diag(K)* Dl + diag(kr)* D3;
```

The convergence results for the three discretization methods are shown in Fig. 5. We plot a discrete L_2 norm of the error in the approximate solution against number of grid points, N. The performance of the Chebyshev spectral method is quite poor for this abrupt solution, while the adaptive scheme reaches a relative error around 10^{-9} already with 200 grid points. The numerical singularities of the solution have real part $\delta = x_\delta$ and the imaginary parts, $\pm\epsilon$, scale like $\epsilon \sim \beta^{-1}$, which is consistent with the scaling properties of the front.

In the context of a linear stability analysis, it is crucial to check the accuracy of the derivatives of the computed solutions, as they are required in the construction of the linearized operator. Fig. 6 shows the convergence history for the first (A), second (B), third (C) and fourth (D) order derivatives of the solution. The convergence plots illustrate one of the challenges of solving PDEs with higher order derivatives using differentiation: numerical differentiation is an unstable operation, and the onset of finite precision effects may pollute the computed derivatives. In our case the accuracy is still sufficient for our computations, but if higher accuracy is required, other techniques such as spectral integration should be pursued [45].

6.2. Results for the model of infiltration

Fig. 7 presents the convergence towards zero of the spectral abscissa associated with $\omega = 0$. As the initial saturation is reduced, the grid spacing required to resolve the wetting front decreases, and the maximum attainable accuracy also reduces. Note, however, that reasonably accurate results can be obtained with a few hundred grid points for saturations as low as $u^+ = 10^{-4}$, which is two orders of magnitude smaller than the typical precursor size used in the thin films literature for analogous stability analyses [26,44]. The effect of conditioning on the accuracy of the scheme is shown in Fig. 8. We plot the condition number of the first-order differentiation matrix, against the error in the spectral abscissa, $|\beta|$. The model parameters and number of grid points coincide with those used in the convergence curves of Fig. 7.

The comparison with standard discretization schemes (Fig. 9) illustrates the power of the proposed adaptive algorithm. The difference between the standard and adaptive algorithms obviously increases as the initial saturation is decreased.

Fig. 10 presents the scaling of the minimum grid spacing, h_{min}, given by the adaptive algorithm, in terms of the initial saturation and flux ratio. We have plotted several realizations with various u^- and u^+. The minimum grid spacing required by the adaptive algorithm seems to behave like $h_{min} \sim u^+(u^-)^{-1.1}$, which is similar to the natural scaling of the small-scale feature downstream of the wetting front.

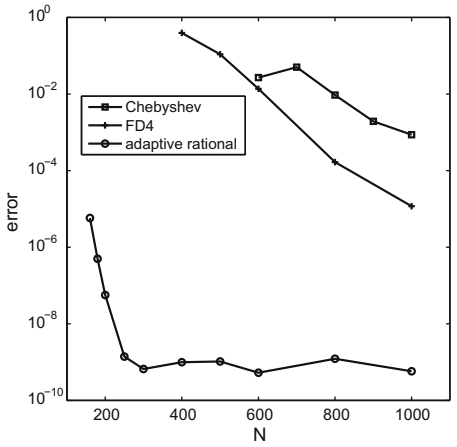

Fig. 5. Convergence results for the test problem (58). We compare the convergence of the adaptive rational scheme with that of the Chebyshev spectral method and fourth-order centered differences.

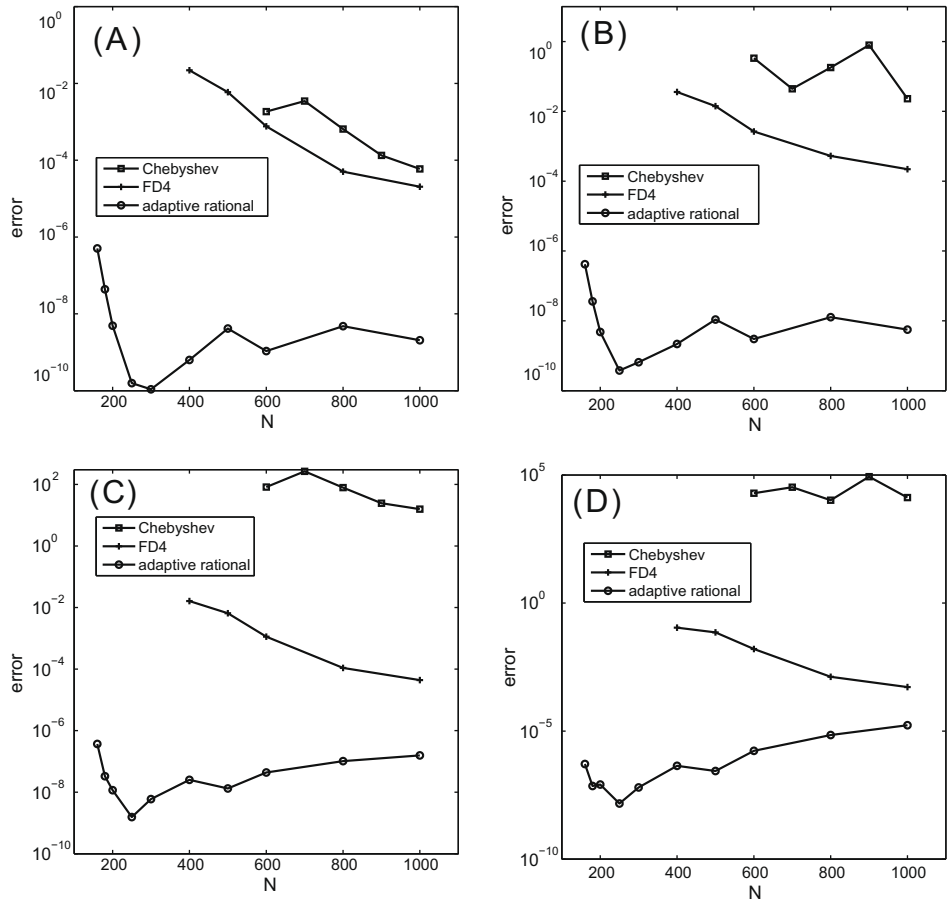

Fig. 6. Convergence results for the test problem (58). Results for the derivatives of the solution. We compare the convergence of the adaptive rational scheme with that of the Chebyshev spectral method and fourth-order centered differences. (A) First-order derivative. (B) Second-order derivative. (C) Third-order derivative. (D) Fourth-order derivative.

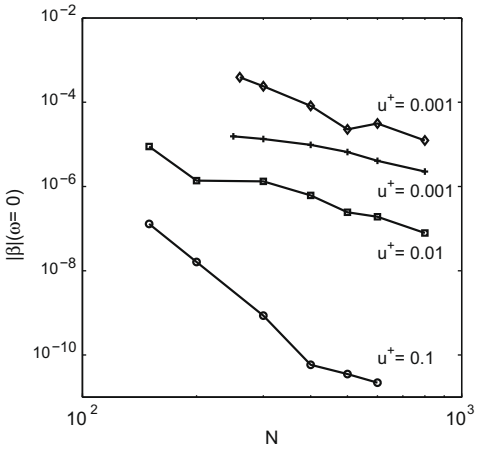

Fig. 7. Convergence of the spectral abscissa, $|\beta|$, for $\omega = 0$ and various initial saturations, u^+, using the adaptive rational spectral method.

Fig. 11 presents some results of the stability analysis using the adaptive rational scheme. Fig. 11A compares the traveling wave solutions for several values of the initial water saturation, which illustrates the importance of this parameter on the saturation overshoot. The location of the singularities of the traveling wave solutions of Fig. 11A is depicted in Fig. 11C.

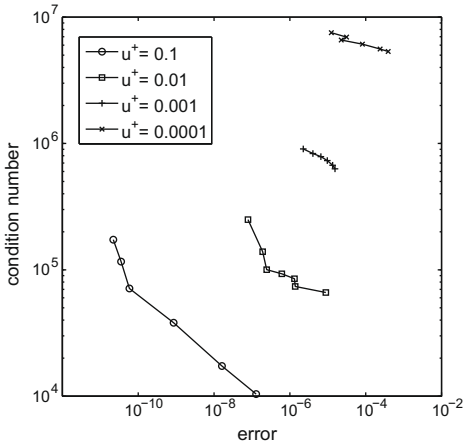

Fig. 8. Condition number of the first-order differentiation matrix against error in the spectral abscissa, $|\beta|$, for various initial saturations, u^+, using the adaptive rational spectral method. The model parameters and number of grids points are the same ones used in the convergence curves of Fig. 7.

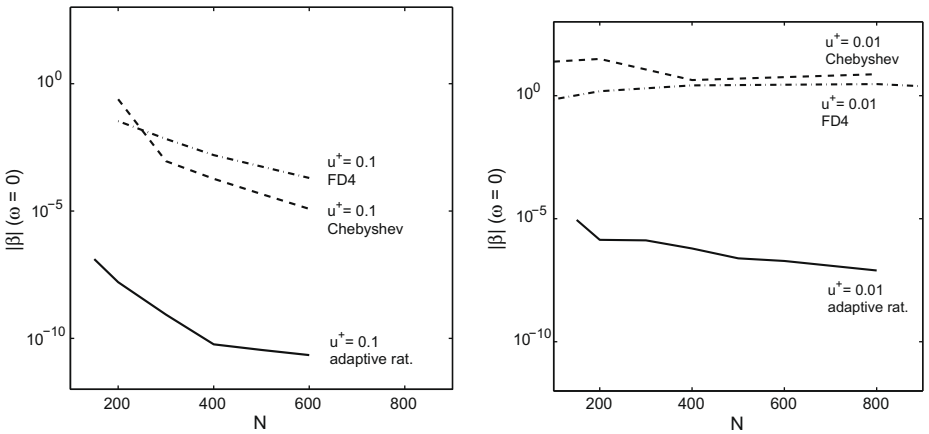

Fig. 9. Convergence of the spectral abscissa, $|\beta|$, for $\omega = 0$. We compare the adaptive rational spectral method and standard collocation schemes. Left, $u^+ = 0.1$. Right, $u^+ = 0.01$.

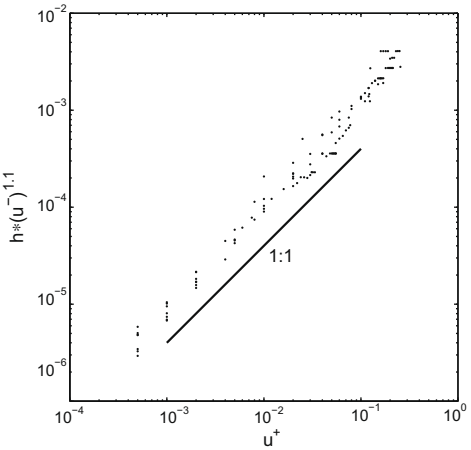

Fig. 10. Scaling of the minimum grid spacing, h_{min}, given by the adaptive algorithm, in terms of the initial saturation and flux ratio. The dots represent realizations corresponding to different values of the initial saturation u^+ and infiltrating flux $k_r(u^-)$. In all cases we use $n = 10$, $N_{gr} = 1$, and $N\ell = 1$.

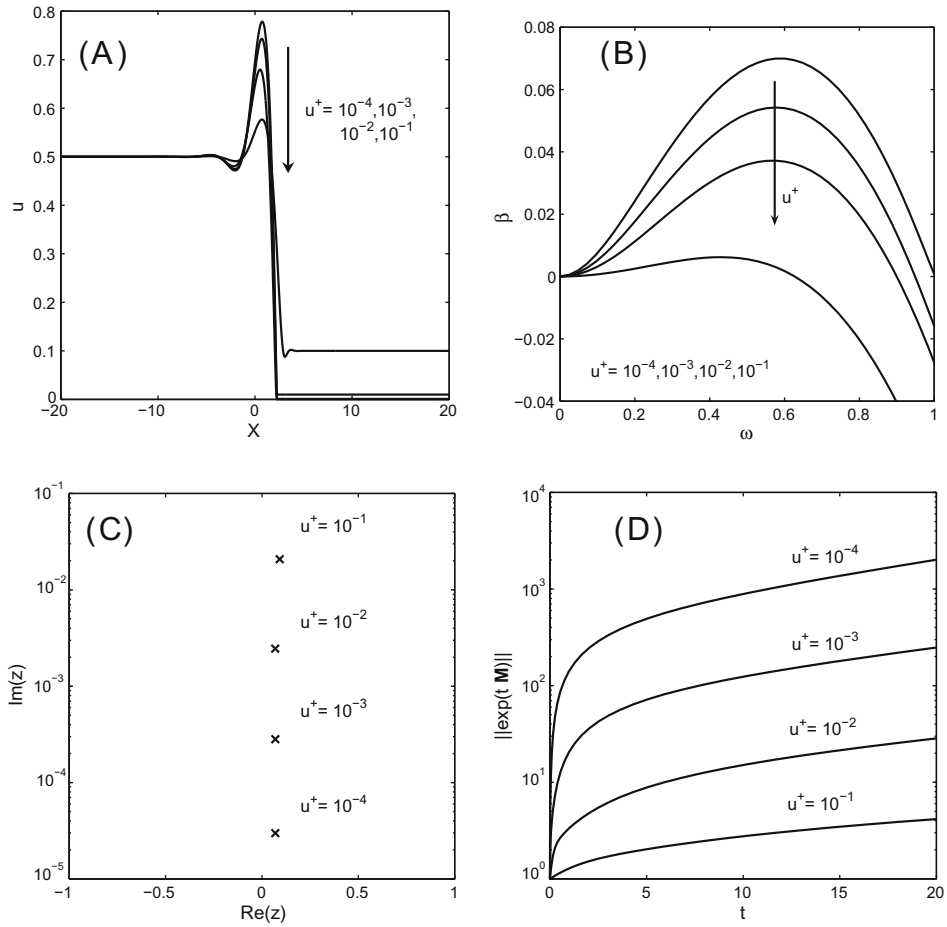

Fig. 11. Results of the stability analysis using the adaptive rational method. (A) Traveling wave solutions for almost dry media. The imaginary part of the singularities, ϵ, scales like u^+ (C). The initial water saturation plays a critical role in the instability of the wetting front, as illustrated by the dispersion curves (B) and transient growth (D) for different values of u^+.

The movement of the real part as u^+ decreases reflects the increased sharpness of the front, while the scaling of the imaginary parts ($\epsilon \sim u^+$) is consistent with the scaling of the wetting front features.

The impact of the initial saturation on the size of the overshoot is also a measure of its impact on the stability of the wetting front, as shown in Fig. 11B. The dispersion curves reveal a fast decay of the growth factors as the initial saturation is increased. Note also that, for sufficiently dry media, the frequency of the most unstable mode ($\sim d_f^{-1}$, where d_f is the finger width) is almost insensitive to changes in u^+. For larger values of the initial saturation the finger width increases, until the front is stabilized. The stabilization of the wetting front for larger values of u^+ also correlates with milder transient growth, as shown in Fig. 11D. Complete details of the conclusions of a linear stability analysis of the proposed model of infiltration are given in [25].

7. Conclusions

We present an adaptive rational spectral method for nonlinear, fourth-order equations, and apply it to the linear stability analysis of a newly proposed model of infiltration into soil [24,25], which explains the formation of "gravity fingers", as observed in the experiments. One of the key components of the linear stability analysis is the accurate computation of the base state (a traveling wave). For small values of the initial water saturation, which are precisely the interesting cases, the sharpness and complex structure of the wetting front preclude the use of the standard Chebyshev pseudo-spectral method, which exhibits very slow convergence rates. In addition, the presence of fourth-order derivatives renders the numerical treatment of the model quite challenging, due to the explosive growth of the condition number of the Chebyshev differentiation matrices, and the associated finite precision effects. We discuss the effectiveness and conditioning of the proposed adaptive discretization, and show that it allows the computation of accurate traveling waves and eigenvalues for small values of the initial water saturation/film precursor, outperforming existing approaches for the linear stability analysis of similar equations [18,26,44].

The linear stability analysis reveals the fundamental role of the saturation overshoot in the onset of the wetting front instability [25], in accordance with experiments. Also consistent with experimental measurements is the critical role of the initial water saturation: larger initial saturations lead to smaller growth factors and transient growth, correlating with the stabilization of the wetting front for increasing initial water content.

The numerical formulation presented here has direct applicability to the flow of thin films, and we anticipate that it will prove instrumental for the stability analysis of other phase-field models of multiphase flow in porous media we are currently developing.

Acknowledgments

We gratefully acknowledge funding for this research, provided by Eni under the Multiscale Reservoir Science project, and by the ARCO Career Development Chair.

References

[1] A. Babchin, I. Brailovsky, P. Gordon, G. Sivashinsky, Fingering instability in immiscible displacement, Phys. Rev. E 77 (2008) 026301.
[2] R. Baltensperger, J.-P. Berrut, The linear rational collocation method, J. Comput. Appl. Math. 134 (2001) 243–258.
[3] R. Baltensperger, J.-P. Berrut, B. Noël, Exponential convergence of a linear rational interpolant between transformed Chebyshev points, Math. Comput. 68 (1999) 1109–1120.
[4] T.W.J. Bauters, D.A. DiCarlo, T.S. Steenhuis, J.-Y. Parlange, Soil water content dependent wetting front characteristics in sands, J. Hydrol. 231 (2000) 244–254.
[5] A. Bayliss, A. Class, B.J. Matkowsky, Roundoff error in computing derivatives using the Chebyshev differentiation matrix, J. Comput. Phys. 116 (1995) 380–383.
[6] A. Bayliss, B.J. Matkowsky, Fronts, relaxation oscillations and period doubling in solid fuel combustion, J. Comput. Phys. 71 (1987) 147–168.
[7] A. Bayliss, E. Turkel, Mappings and accuracy for Chebyshev pseudo-spectral approximations, J. Comput. Phys. 101 (1992) 349–359.
[8] J. Bear, Dynamics of Fluids in Porous Media, Elsevier, New York, 1972.
[9] J.-P. Berrut, Rational functions for guaranteed and experimentally well-conditioned global interpolation, Math. Comput. 15 (1988) 1–16.
[10] J.-P. Berrut, The barycentric weights of rational interpolation with prescribed poles, J. Comput. Appl. Math. 86 (1997) 45–52.
[11] J.-P. Berrut, R. Baltensperger, The linear rational pseudospectral method for boundary value problems, BIT 41 (2001) 868–879.
[12] J.-P. Berrut, H.D. Mittelmann, Lebesgue constant minimizing linear rational interpolation of continuous functions over the interval, Comput. Math. Appl. 33 (1997) 77–86.
[13] J.-P. Berrut, H.D. Mittelmann, Rational interpolation through the optimal attachment of poles to the interpolating polynomial, Numer. Algor. 23 (2000) 315–328.
[14] J.-P. Berrut, H.D. Mittelmann, The linear rational pseudospectral method with iteratively optimized poles for two-point boundary value problems, SIAM J. Sci. Comput. 23 (2001) 961–975.
[15] J.-P. Berrut, H.D. Mittelmann, Adaptive points shifts in rational approximation with optimized denominator, J. Comput. Appl. Math. 164 (2004) 81–92.
[16] J.-P. Berrut, H.D. Mittelmann, Optimized points shifts and poles in the linear rational pseudospectral method for boundary value problems, J. Comput. Phys. 204 (2005) 292–301.
[17] J.-P. Berrut, L.N. Trefethen, Barycentric Lagrange interpolation, SIAM Rev. 46 (2004) 501–517.
[18] A.L. Bertozzi, M.P. Brenner, Linear stability and transient growth in driven contact lines, Phys. Fluids 9 (1997) 530–539.
[19] W.J. Boettinger, J.A. Warren, C. Beckermann, A. Karma, Phase-field simulation of solidification, Annu. Rev. Mater. Res. 32 (2002) 163–194.
[20] J.P. Boyd, Why Newton's method is hard for traveling waves: small denominators, KAM theory, Arnold's linear Fourier problem, non-uniqueness, constraints and erratic failure, Math. Comput. Simul. 74 (2007) 72–81.
[21] J.W. Cahn, On spinodal decomposition, Acta Met. 9 (1961) 795–801.
[22] J.W. Cahn, J.E. Hilliard, Free energy of non-uniform systems. I. Interfacial free energy, J. Chem. Phys. 28 (1958) 258–267.
[23] R.L. Chuoke, P. van Meurs, C. van der Poel, The instability of slow immiscible viscous liquid–liquid displacements in permeable media, Petrol. Trans. Am. Inst. Min. Eng. 216 (1959) 188–194.
[24] L. Cueto-Felgueroso, R. Juanes, Nonlocal interface dynamics and pattern formation in gravity-driven unsaturated flow through porous media, Phys. Rev. Lett. 101 (2008) 244504.
[25] L. Cueto-Felgueroso, R. Juanes, Linear stability analysis of a phase-field model of gravity-driven unsaturated flow in porous media, Phys. Rev. E 79 (2009) 036301.
[26] J.M. Davis, D.E. Kataoka, S.M. Troian, Transient dynamics and structure of optimal excitations in thermocapillary spreading: precursor film model, Phys. Fluids 18 (2006) 092101.
[27] J.M. Davis, S.M. Troian, On a generalized approach to the linear stability of spatially nonuniform thin film flows, Phys. Fluids 15 (2003) 1344–1347.
[28] P.G. de Gennes, Wetting: statics and dynamics, Rev. Mod. Phys. 57 (1985) 827–863.
[29] J. Van Deun, K. Deckers, A. Bultheel, J.A.C. Weideman, Near-best fixed pole rational interpolation with applications in spectral methods, ACM Trans. Math. Software 35 (2008). Art. No. 14.
[30] D.A. DiCarlo, Experimental measurements of saturation overshoot on infiltration, Water Resour. Res. 40 (2004) W04215.
[31] D.A. DiCarlo, Capillary pressure overshoot as a function of imbibition flux and initial water content, Water Resour. Res. 43 (2007) W08402.
[32] D.A. DiCarlo, M.J. Blunt, Determination of finger shape using the dynamic capillary pressure, Water Resour. Res. 36 (9) (2000) 2781–2785.
[33] G.A. Diment, K.K. Watson, Stability analysis of water movement in unsaturated porous materials 2. Numerical studies, Water Resour. Res. 19 (1983) 1002–1010.
[34] G.A. Diment, K.K. Watson, Stability analysis of water movement in unsaturated porous materials 3. Experimental studies, Water Resour. Res. 21 (1985) 979–984.
[35] G.A. Diment, K.K. Watson, P.J. Blennerhassett, Stability analysis of water movement in unsaturated porous materials 1. Theoretical considerations, Water Resour. Res. 18 (1982) 1248–1254.
[36] X. Du, T. Yao, W.D. Stone, J.M.H. Hendrickx, Stability analysis of the unsaturated water flow equation 2. Experimental verification, Water Resour. Res. 37 (2001) 1875–1881.
[37] A.G. Egorov, R.Z. Dautov, J.L. Nieber, A.Y. Seshukov, Stability analysis of gravity-driven infiltrating flow, Water Resour. Res. 39 (2003) 1266.
[38] M. Eliassi, R.J. Glass, On the continuum-scale modeling of gravity-driven fingers in unsaturated porous media: the inadequacy of the Richards equation with standard monotonic constitutive relations and hysteretic equations of state, Water Resour. Res. 37 (2001) 2019–2035.
[39] M. Eliassi, R.J. Glass, On the porous-continuum modeling of gravity-driven fingers in unsaturated materials: Extension of the standard theory with a hold-back-pile-up effect, Water Resour. Res. 38 (2002) 1234.
[40] H. Emmerich, Advances of and by phase-field modelling in condensed-matter physics, Adv. Phys. 57 (2008) 1–87.
[41] M.S. Floater, K. Hormann, Barycentric rational interpolation with no poles and high rates of approximation, Numer. Math. 107 (1993) 315–331.

[42] S.L. Geiger, D.S. Durnford, Infiltration in homogeneous sands and a mechanistic model of unstable flow, Soil Sci. Soc. Am. Proc. 64 (2000) 460–469.
[43] R.J. Glass, J.-Y. Parlange, T.S. Steenhuis, Wetting front instability 2. Experimental determination of relationships between system parameters and two-dimensional unstable flow field behaviour in initially dry porous media, Water Resour. Res. 25 (1989) 1195–1207.
[44] J.M. Gomba, J. Diez, R. Gratton, A.G. Gonzalez, Stability study of a constant-volume thin film flow, Phys. Rev. E 76 (2007) 046308.
[45] L. Greengard, Spectral integration and two-point boundary value problems, SIAM J. Numer. Anal. 28 (1991) 1071–1080.
[46] H.P. Greenspan, On the motion of a small viscous droplet that wets a surface, J. Fluid Mech. 84 (1978) 125–143.
[47] H. Guillard, R. Peyret, On the use of spectral methods for the numerical solution of stiff problems, Comput. Methods Appl. Mech. Eng. 66 (1988) 17–43.
[48] D. E Hill, J.-Y. Parlange, Wetting front instability in homogeneous soils, Soil Sci. Soc. Am. Proc. 36 (1972) 697–702.
[49] L.M. Hocking, Spreading and instability of a viscous fluid sheet, J. Fluid Mech. 211 (1990) 373–392.
[50] H.E. Huppert, Flow and instability of a viscous current down a slope, Nature 300 (1982) 427–429.
[51] V. Kapoor, Criterion for instability of steady-state unsaturated flows, Transport Porous Med. 25 (1996) 313–334.
[52] L. Kondic, A.L. Bertozzi, Nonlinear dynamics and transient growth of driven contact lines, Phys. Fluids 11 (1999) 3560–3562.
[53] L. Kondic, J. Diez, Flow of thin films on patterned surfaces: controlling the instability, Phys. Rev. E 65 (2002) 045301.
[54] D. Kosloff, H. Tal-Ezer, A modified Chebyshev pseudospectral method with an $O(N^{-1})$ time step restriction, J. Comput. Phys. 104 (1993) 457–469.
[55] R. Lenormand, Pattern growth and fluid displacements through porous media, Physica A 140 (1986) 114–123.
[56] R. Lenormand, E. Touboul, C. Zarcone, Numerical models and experiments on immiscible displacements in porous media, J. Fluid Mech. 189 (1988) 165–187.
[57] M.C. Leverett, Capillary behavior of porous solids, Petrol. Trans. Am. Inst. Min. Eng. 142 (1941) 52–169.
[58] G. Løvoll, Y. Méheust, R. Toussaint, J. Schmittbuhl, K.J. Måløy, Growth activity during fingering in a porous Hele–Shaw cell, Phys. Rev. E 70 (2004) 026301.
[59] T.X. Lu, J.W. Biggar, D.R. Nielsen, Water movement in glass bead porous media 2. Experiments of infiltration and finger flow, Water Resour. Res. 30 (1994) 3283–3290.
[60] Y. Mualem, A new model for predicting the hydraulic conductivity of unsaturated porous media, Water Resour. Res. 12 (3) (1976) 513–522.
[61] J.L. Nieber, R.Z. Dautov, A.G. Egorov, A.Y. Sheshukov, Dynamic capillary pressure mechanism for instability in gravity-driven flows; review and extension to very dry conditions, Transport Porous Med. 58 (2005) 147–172.
[62] J.-Y. Parlange, D.E. Hill, Theoretical analysis of wetting front instability in soils, Soil Sci. 122 (1976) 236–239.
[63] J.R. Philip, Theory of infiltration, in: V.T. Chow (Ed.), Advances in Hydroscience, Academic Press, New York, 1969, pp. 215–296.
[64] J.R. Philip, Stability analysis of infiltration, Soil Sci. Soc. Am. Proc. 39 (1975) 1042–1049.
[65] A. Riaz, H.A. Tchelepi, Numerical simulation of immiscible two-phase flow in porous media, Phys. Fluids 18 (2006) 014104.
[66] L.A. Richards, Capillary conduction of liquids through porous mediums, Physics 1 (1931) 318–331.
[67] P.G. Saffman, G.I. Taylor, The penetration of a fluid into a porous medium or Hele–Shaw cell containing a more viscous fluid, Proc. Roy. Soc. Lond. 245 (1958) 312–329.
[68] M. Sahimi, Flow phenomena in rocks – from continuum models to fractals, percolation,cellular-automata, and simulated annealing, Rev. Mod. Phys. 65 (4) (1993) 1393–1534.
[69] J.S. Selker, P. Leclerq, J.-Y. Parlange, T.S. Steenhuis, Fingered flow in two dimensions 1. Measurement of matric potential, Water Resour. Res. 28 (1992) 2513–2521.
[70] J.S. Selker, J.-Y. Parlange, T.S. Steenhuis, Fingered flow in two dimensions 2. Predicting finger moisture profile, Water Resour. Res. 28 (1992) 2523–2528.
[71] S. Shiozawa, H. Fujimaki, Unexpected water content profiles under flux-limited one-dimensional downward infiltration in initially dry granular media, Water Resour. Res. 40 (2004) W07404.
[72] O.T.N. Sililo, J.H. Tellam, Fingering in unsaturated zone flow: a qualitative review with laboratory experiments in heterogeneous systems, Ground Water 38 (2000) 864–871.
[73] T.W. Tee, An adaptive rational spectral method for differential equations with rapidly varying solutions. Ph.D. Thesis, vol. 28, 2006, pp. 1798–1811.
[74] T.W. Tee, L.N. Trefethen, A rational spectral collocation method with adaptively transformed Chebyshev grid points, SIAM J. Sci. Comput. 28 (2006) 1798–1811.
[75] N. Tiwari, Z. Mester, J.M. Davis, Stability and transient dynamics of thin liquid films flowing over locally heated surfaces, Phys. Rev. E 76 (2007) 056306.
[76] L.N. Trefethen, Spectral Methods in Matlab, Society for Industrial and Applied Mathematics (SIAM), 2000.
[77] S.M. Troian, E. Herbolzheimer, S.A. Safran, J.F. Joanny, Fingering instabilities of driven spreading films, Phys. Fluids 10 (1989) 25–30.
[78] N. Ursino, Linear stability analysis of infiltration analytical and numerical solution, Transport Porous Med. 38 (2000) 261–271.
[79] C.J. van Duijn, G.J.M. Pieters, P.A.C. Raats, Steady flows in unsaturated soils are stable, Transport Porous Med. 57 (2004) 215–244.
[80] M.T. van Genuchten, A closed form equation to predict the water conductivity of unsaturated soil, Soil Sci. Soc. Am. Proc. 44 (1980) 892–898.
[81] Z. Wang, W.A. Jury, A. Tuli, D.-J. Kim, Unstable flow during redistribution: controlling factors and practical implications, Vadose Zone J. 3 (2004) 549–559.
[82] Z. Wang, A. Tuli, W.A. Jury, Unstable flow during redistribution in homogeneous soil, Vadose Zone J. 2 (2003) 52–60.
[83] J.A.C. Weideman, Computing the dynamics of complex singularities of nonlinear PDEs, SIAM J. Appl. Dyn. Syst. 2 (2003) 171–186.
[84] J.A.C. Weideman, L.N. Trefethen, The eigenvalues of second-order spectral differentiation matrices, SIAM J. Numer. Anal. 25 (1988) 1279–1298.
[85] D.A. Weitz, J.P. Stokes, R.C. Ball, A.P. Kushnick, Dynamic capillary pressure in porous media: origin of the viscous fingering lengthscale, Phys. Rev. Lett. 59 (1987) 2967–2970.
[86] L. Zhornitskaya, A.L. Bertozzi, Positivity-preserving numerical schemes for lubrication-type equations, SIAM J. Numer. Anal. 37 (2000) 523–555.